September 9, 2015

The opportunity offered by the ESSnuSB project to exploit the larger leptonic CP violation signal at the second oscillation maximum and the requirements of this project on the ESS accelerator complex

E. Wildner, M. Martini, H. Schönauer, CERN, Geneva, Switzerland,
A. Burgman, J. Cederkäll, P. Christiansen, Lund University, Lund, Sweden,
T. Ekelöf, M. Olvegård, Uppsala University, Uppsala, Sweden,
for ESSnuSB.

Abstract

Very intense neutrino beams and large neutrino detectors will be needed to enable the discovery of CP violation in the leptonic sector. The production of such neutrino beams requires very powerful proton drivers. The European Spallation Source (ESS), currently under construction in Lund, Sweden, is a research center that will provide, by 2023, the world's most powerful neutron source. The ESS proton linac will accelerate more than 10^{15} protons to 2.0 GeV (originally planned energy 2.5 GeV) in 2.86 ms long pulses at 14 Hz and send this proton beam onto the spallation target. The instantaneous power will be 125 MW and the average power 5 MW. Pulsing this linac at higher frequency, at the same instantaneous power, will make it possible to raise the average beam power to 10 MW to produce, in parallel with the spallation neutron production, a very intense, cost effective and high performance neutrino Super Beam of about 0.4 GeV mean neutrino energy.

From the value of the neutrino mixing angle θ_{13} measured in 2012 it follows that the CP violation sensitivity at the second neutrino oscillation maximum is significantly larger than at the first. The ESS neutrino Super Beam, ESSnuSB, operated with a 2.0 GeV (2.5 GeV) linac proton beam, together with a large underground Water Cherenkov detector located in Garpenberg, at 540 km from Lund, close to the second oscillation maximum, will make it possible to discover leptonic CP violation at 5 σ significance level in 56% (65%) of the leptonic Dirac CP-violating phase range after 10 years of data taking and 69% (71%) after 20 years of data taking. To obtain similar performance at the first oscillation maximum, an error level of 1-3% would be necessary - the realism of which remains to be proven.

The paper gives an overview of the proposed facility and, in particular, presents the outstanding physics reach possible for CP violation with ESSnuSB. The upgrades and developments of the ESS accelerator facility required for ESSnuSB are described. Special attention is given to the comparatively modest modifications of the linac design that need to be made during the linac build-up phase 2017-2023 in order to significantly simplify and reduce the cost and time for the subsequent linac upgrade enabling production of a neutrino beam. A detailed description is given of the design considerations for the beam accumulator ring. The design requirements for the Near Detector are discussed and results of some simulation studies of a preliminary design of that detector are reported.

1 Overview

Previous designs of high performance "Neutrino Factories" to discover CP violation in the leptonic sector, were made assuming a very low value of the until then unknown neutrino mixing angle θ_{13}. Recent measurements of θ_{13} [1–4] show that this angle is large, making it possible to measure CP violation in the leptonic sector using high power conventional "Super Beams". The large value of θ_{13} furthermore implies that that the sensitivity to CP violation is significantly higher at the second neutrino oscillation maximum as compared to the first.

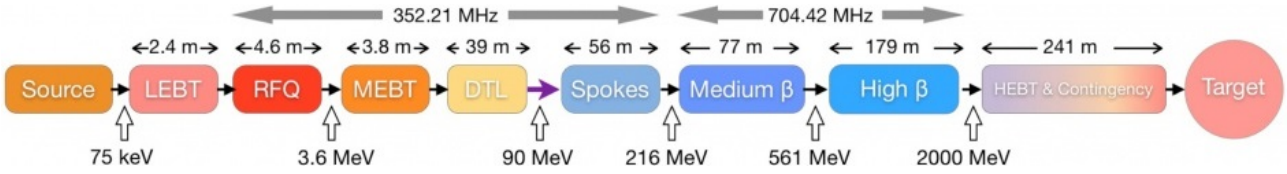

Figure 1: The ESS superconducting linac

The European Spallation Source (ESS) [5] under construction in Lund, Sweden since fall of 2014, is a research centre that will have the world's most powerful neutron source. It is based on a 2.0 GeV superconducting linac (originally planned energy 2.5 GeV), giving 2.86 ms long proton pulses at 14 Hz for the spallation facility with 5 MW average power on target (Fig. 1). By pulsing the linac at higher frequency, additional beam pulses can be interleaved to provide a total average beam power of 10 MW. The extra pulses, each providing 1.1 10^{15} protons on target, corresponding to 2.7 10^{23} protons on target per year, can be used to obtain a neutrino beam of unprecedented intensity. The uniquely high intensity of the ESS linac allows the positioning of the ESSnuSB detector at the second neutrino oscillation maximum, where the relative CP violation sensitivity is about three times higher than at the first maximum, where the DUNE experiment in the US [6] and the Hyper-K experiment in Japan [7] have their respective detectors positioned.

The European Spallation Source neutrino Super Beam project, ESSnuSB [8], proposes to use the Super Beam described above to search for leptonic CP violation. The detector will be located in the 1200 m deep Garpenberg mine located at a distance of 540 km from the neutrino source in Lund, near the second neutrino oscillation maximum. Table 1 shows an overview of the parameters of the facility. The ESSnuSB Design Study is taking advantage of many of the results obtained in the FP7 Design Study EUROnu [9] on future neutrino facilities. The results from the now terminated EUROnu project of the study of the 4.5 GeV / 5 MW neutrino Super Beam from the CERN Superconducting Proton Linac SPL [10, 11] and of the MEMPHYS large Water Cherenkov detector in the Fréjus tunnel, have served as very useful references in the ESSnuSB Design Study [12, 13].

Parameter	**Value**
Average neutrino energy	0.36 GeV
Baseline	540 km
Detector technology	Water Cherenkov
Fiducial volume	500 kt
PMTs	240k 8"
10 year reach (8ν+$2\bar{\nu}$)	60% of δ_{cp} range (5 σ)
L/E (2^{nd} oscillation max.)	1500 km/GeV

Table 1: Main parameters of the ESSnuSB neutrino facility

The purpose of ESS is the production and use of spallation neutrons. The use of the ESS linac for neutron and neutrino production simultaneously, not reducing neutron production, will decrease considerably the cost of the proposed neutrino project as compared to constructing a dedicated proton driver for generating the neutrino

beam. The current main parameters of the ESS proton driver are listed in table 2.

Parameter	**Value**
Average Beam Power	5 MW
Ion kinetic energy	2 GeV
Average macro pulse current	62.5 mA
Average macro pulse length	2.86/4 ms
Pulse repetition rate	14 Hz
Maximum accelerating cavity surface field	45 MV/m
Linac length	352.5 m
Reliability	95%
Annual operating period	5000 h

Table 2: Current main parameters of the ESS linac.

With presently available technology, the horn-type hadron collector cannot handle 2.86 ms long pulses due to the excessive ohmic heating of the magnet-system current-leads. Therefore, the linac pulse has to be accumulated in a multi-turn injection storage ring that can deliver, through single turn extraction, pulses of a few μs length to the neutrino production target and horn assembly. There is space available on the ESS site to implement such a proton accumulator and its transfer lines from the linac and to the target station as well as for the target station itself and a Near Detector. To inject protons from the linac into the accumulator with satisfactory efficiency, charge exchange injection will be necessary. Therefore, the ESS linac has to be further equipped such that it can be used to accelerate H^- pulses of the same length and intensity as the proton pulses.

A preliminary study of the modifications of the ESS linac that are required to allow simultaneous acceleration of H^+ and H^- ions at an average power of 5+5 MW has been made [14]. It is important that some of these modifications be made already during the linac construction phase, such that it will later be possible to upgrade the linac without interventions that would disrupt the use of the linac for the production of spallation neutrons and significantly increase the cost and the time required for the upgrade.

The proposed upgrade of the accelerator complex will significantly increase the potential and options also for other future developments of the ESS. One example of this is that the accumulator studies aim at a design allowing the accumulator to satisfy the requirements for the production of both short neutrino pulses of ca 1.5 microsecond length through single turn extraction and short neutron pulses of the order of 100 μs length through multi-turn extraction, thus also providing, as a future option, the production of short, uniquely intense neutron pulses [15].

The EUROnu studies identified some key elements of the SPL Super Beam for which further R&D would be necessary, such as the proton target, the hadron collector and its pulse generator. These items will be further studied to prove their feasibility for the ESS based neutrino project. Simulation studies of the optimal distance for a 2.0 to 3 GeV proton beam have resulted in the choice of the 1200 m deep Garpenberg mine in the Swedish Dalarna county, 540 km from ESS in Lund, as the optimal location for the Far Neutrino Detector. The Near Detector will contain a Water Cherenkov detector and possibly other types of detectors. Results from the European FP7 LAGUNA Design Study [16] provide useful information for the design of the detectors and the needed infrastructure.

2 The significant advantage of measuring leptonic CP violation at the second oscillation maximum

The physics of the ESSnuSB, having its detector at the second oscillation maximum, will be discussed using the expression for the probability for the $\nu_\mu \rightarrow \nu_e$ oscillation, written in the formula below:

$$\begin{aligned} P(\nu_\mu \rightarrow \nu_e) = & \sin^2\theta_{23}\sin^2 2\theta_{13}\sin^2\left(\frac{\Delta_{31}L}{2}\right) \\ & + \cos^2\theta_{23}\sin^2 2\theta_{12}\sin^2\left(\frac{\Delta_{21}L}{2}\right) \\ & + \widetilde{J}\cos\left(\delta_{cp} - \frac{\Delta_{31}L}{2}\right)\sin\left(\frac{\Delta_{21}L}{2}\right)\sin\left(\frac{\Delta_{31}L}{2}\right) \end{aligned}$$

where $\widetilde{J} \equiv \cos\theta_{13}\sin 2\theta_{12}\sin 2\theta_{23}\sin 2\theta_{13}$ and $\Delta_{ij} \equiv \frac{\Delta m^2_{ij}}{2E_\nu}$. The sign of δ_{cp} is the opposite for antineutrinos.

The first two terms in this expression are generally referred to as the "atmospheric" term and the "solar" term respectively. The third is the "CP interference" term which is the only term that depends on the CP violating angle δ_{cp} [17].

Plots for two different values of the mixing angle, θ_{13} = 1 ° and θ_{13} = 10 °, of the three terms in the $\nu_\mu \rightarrow \nu_e$ oscillation probability expression are shown in Fig. 2 as a function of the variable L/E, the ratio between the accelerator-detector distance L (the base line) and the neutrino energy E. The CP-violating term is calculated without the factor $cos\left(\delta_{cp} - \frac{\Delta_{31}L}{2}\right)$, i.e. what is shown is the maximum value this term could take on. The first and second neutrino oscillation maxima are clearly seen in the atmospheric term to be at L/E = 500 km/GeV and 1500 km/GeV.

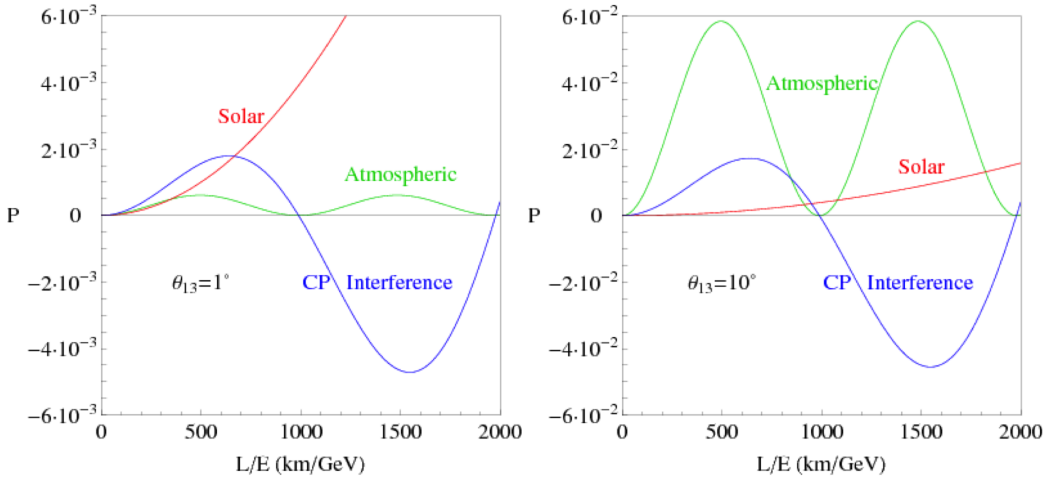

Figure 2: Plots showing, for two different values of the neutrino mixing angle θ_{13} = 1 ° (left panel) and θ_{13} = 10 ° (right panel), the three terms in the expression for the $\nu_\mu \rightarrow \nu_e$ oscillation probability as function of the ratio between the accelerator to detector distance L (the base line) and the neutrino energy E [17]. The CP-violating term is calculated without the factor $\cos\left(\delta_{cp} - \frac{\Delta_{31}L}{2}\right)$, i.e. what is shown is the maximum value this term could take on.

The information on δ_{cp} is thus contained in the CP interference term. As can be seen in the left panel of Fig. 2, for a value of the neutrino mixing angle θ_{13} that is small, like 1 °, which was assumed to be the case before 2012, the CP Interference term has at L/E = 500km/GeV approximately the same magnitude as the solar term and is larger than the atmospheric term whereas at L/E = 1500 km/GeV the CP Interference term is much

smaller than the dominant solar term. Had the value of θ_{13} indeed been small, the sensitivity to δ_{cp} would thus have been much higher at L/E = 500 km/GeV than at L/E = 1500 km/GeV. This was certainly one reason why some proposed projects, which were designed well before 2012, have their respective detectors placed at a distance from the accelerator approximately corresponding to L/E = 500 km/GeV, i.e. at the first maximum. However, when in 2012 θ_{13} was measured to be about 9° [1–4] and thus found to be much larger than what had been expected, the relation between the three terms was drastically changed as shown in the right panel of Fig. 2. For $\theta_{13} = 10^\circ$, the CP interference term at L/E = 500 km/GeV is much smaller than the dominant atmospheric term, whereas it has about the same amplitude as the dominant atmospheric term at L/E = 1500 km/GeV. It is thus clear from these considerations that the sensitivity to δ_{cp} indeed is significantly higher at the second neutrino oscillation maximum than at the first.

The conceptual design of ESSnuSB [8] was made in 2012 and in view of the, at the time, newly measured high value of θ_{13}, the detector was placed at the location of the second neutrino oscillation maximum. For an ESSnuSB proton energy of 2.0 GeV the mean neutrino energy is 360 MeV and the distance of the second maximum from the ν_μ source is of the order of 500 km. Fig. 3 shows, for this baseline, the number of electron neutrinos detected in two years running with positive polarity in the horn as function of neutrino energy E for 4 different values of δ_{cp}: 0 and π, which correspond to no CP violation, and $\pi/2$ and $3\pi/2$, which correspond to maximum CP violation of opposite signs, respectively.

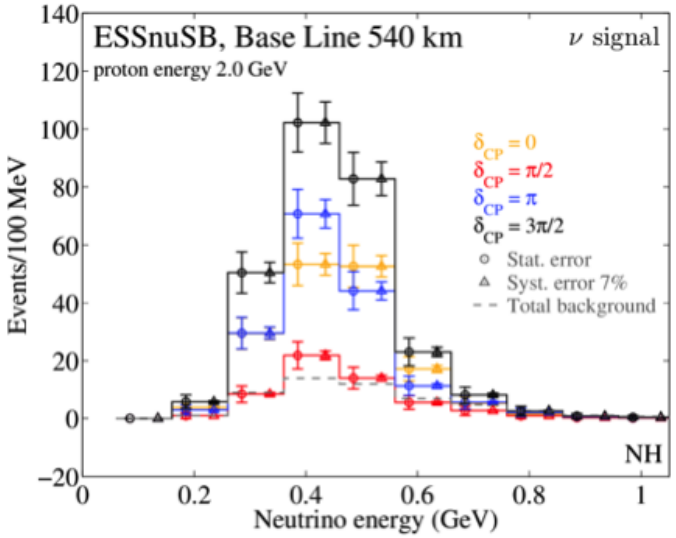

Figure 3: Histograms showing, for a base line of 540 km and a proton energy of 2.0 GeV, the energy distribution for the electron neutrinos detected during 2 years of data taking for 3 different values of δ_{cp}.

Fig. 4 shows the same type of comparison, this time between DUNE and Hyper-K, designed to measure at the first maximum, and ESSnuSB, designed to measure at the second maximum. The ratio between the numbers of electron neutrinos with $\delta_{cp} = 3\pi/2$ and with $\delta_{cp} = \pi/2$ can be seen to be about 1.5 for DUNE, 1.7 for Hyper-K and as high as about 4.8 for ESSnuSB, i.e. about 3 times higher sensitivity to the value of δ_{cp} as compared to the other two experiments.

The four bins in Fig. 5 show the total number of events detected at the second maximum for neutrinos and antineutrinos and for a proton energy of 2 GeV and 2.5 GeV, respectively. The data collection time is 2 years with neutrinos and 8 years with antineutrinos in order to detect (very) approximately equal numbers of electron neutrinos and antineutrinos. For a proton energy of 2.5 GeV the total number of events can be seen to be somewhat higher than for a 2 GeV proton energy, indicating that the energy originally planned for the ESS project of 2.5 GeV would be more favorable for ESSnuSB than the recently down-scoped value of 2.0 GeV. In

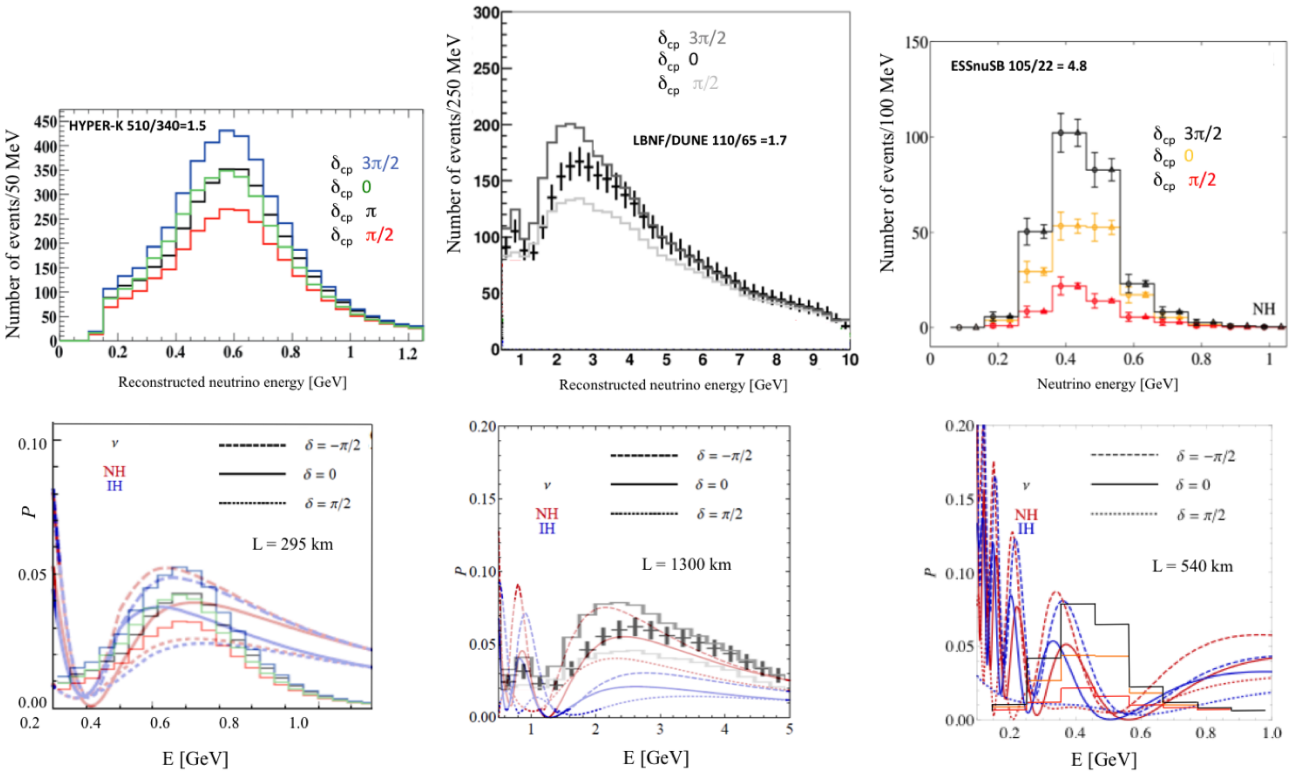

Figure 4: The histograms in the panels in the upper part of the figure show, for the three different neutrino beam projects Hyper-K, DUNE and ESSnuSB, the number of detected electron neutrinos as a function of neutrino energy E for three different values of δ_{cp}: 0, which corresponds to no CP violation, and $\pi/2$ and $3\pi/2$, which correspond to maximum CP violation of opposite signs, respectively. In the lower panels these histograms have been overlaid on the calculated probability for the electron neutrino oscillation for the same three δ_{cp} values, respectively, and for Normal Hierarchy (NH, red) and Inverted Hierarchy (IH, blue), respectively with arbitrary scale for the probability. The ratio between the numbers of electron neutrinos with δ_{cp} = $3\pi/2$ and with $\pi/2$ is noted on each of the upper panels: 4.8 for ESSnuSB and 1.5 and 1.7 respectively for Hyper-K and LBNE/DUNE. This ratio is thus significantly larger for ESSnuSB (measurement at second oscillation maximum) than for Hyper-K and DUNE (measurement at first oscillation maximum).

the future this may be increased in order to increase the neutron intensity.

The T2K experiment [7] has, after nearly 6 years of operation and data analysis managed to reduce its systematic uncertainties for the signal to a level of 7%. Fig. 3 shows, for each 100 MeV bin, the statistical errors as well as a 7% systematic error. The statistical error is seen to be larger than the systematic. However, as shown by the leftmost bar in Fig. 5, which represents the total numbers of events in the histograms in the right panel of Fig. 3, for the total number of events the statistical and systematic errors are in balance. This raises the question of how much information is contained in the relative shape of the histograms in Fig. 3, as this information is not taken into account when considering only the total number of events. The answer to this question may be deduced from the 4 different histograms in Fig. 6, which have been obtained by dividing the 4 histograms of Fig. 3 by their respective total numbers of events. There is some difference between the curves in Fig. 6 but these differences are comparable in magnitude to the statistical errors.

Described so far is what could be done with neutrino beam data collected during 2 years. However, a major goal is to compare the neutrino and antineutrino beam data shown in Fig. 5, which provides additional and very sensitive information on δ_{cp}. Fig. 7 shows for ESSnuSB the normalised difference between the total numbers of

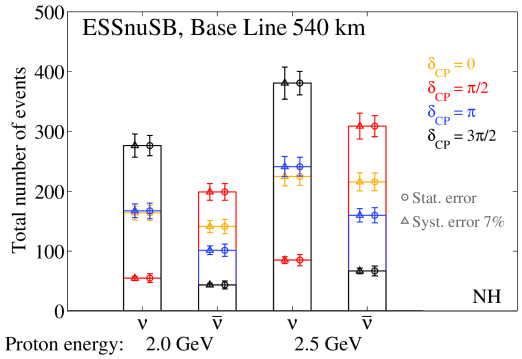

Figure 5: The bins show the total numbers of electron neutrinos and antineutrinos, respectively, detected in ESSnuSB after 2 years of data taking with a neutrino beam and 8 years with an antineutrino beam and for a proton energy of 2.0 GeV and for 2.5 GeV, respectively, with the detector placed at the second maximum.

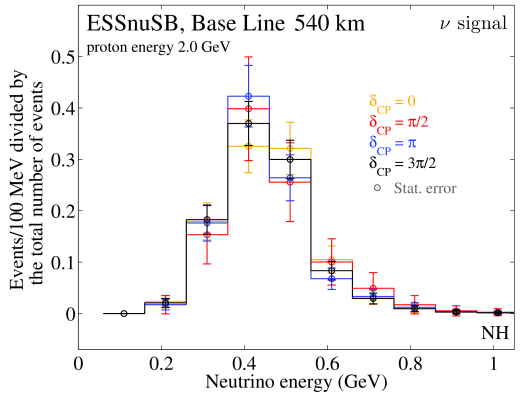

Figure 6: The 4 different histograms in this figure have been obtained by dividing each of the four different histograms in the right panel of Fig. 3 by their respective total numbers of events, so that the difference in relative shape between the histograms can be seen.

electron neutrinos and of electron antineutrinos (Nν_e - N$\overline{\nu}_e$)/(Nν_e +N$\overline{\nu}_e$) for a proton energy of 2.0 GeV and 2.5 GeV, respectively, at the first maximum (left panel) and the second maximum (right panel). The normalization takes into account the difference in the production as well as the detection cross-sections between the neutrinos and the antineutrinos. The variation of the asymmetry with δ_{cp} can be seen to be significantly bigger at the second maximum as compared to the first maximum and the statistical and systematic errors are well balanced. Other investigations of the sensitivity of the neutrino-antineutrino asymmetry to the value of δ_{cp} have shown that the probability P($\overline{\nu}_\mu \rightarrow \overline{\nu}_e$) varies with δ_{cp} between 1/2 and 2 times the probability P($\nu_\mu \rightarrow \nu_e$) at the first maximum and between 1/7 and 7 times the probability P($\nu_\mu \rightarrow \nu_e$) at the second maximum [18].

By fitting simulated [19] ESSnuSB data collected during 2 years with a neutrino beam and 8 years with an antineutrino beam one may calculate the fraction of the total range of possible values for δ_{cp} for which CP violation can be discovered with 5σ and 3σ significance level, respectively. In Fig. 8 is plotted the result of such global calculations for different distances between the accelerator and the detector L from 100 km to 1000 km (horizontal axis), for the three different proton beam energies 2.0, 2.5 and 3.0 GeV (blue, green and red lines, respectively) and for two different values of the mixing angle θ_{13} =4 $^\circ$ (left panel) and θ_{13} =8.73 $^\circ$ (right panel). From these curves one may see that for θ_{13} = 4 $^\circ$ the highest potential for discovery is at the first maximum whereas for θ_{13} = 8.73 $^\circ$ it is at the second maximum. One can also see from the right panel that for the detector being located 540 km from the accelerator the potential is somewhat higher for a proton beam energy of 2.5

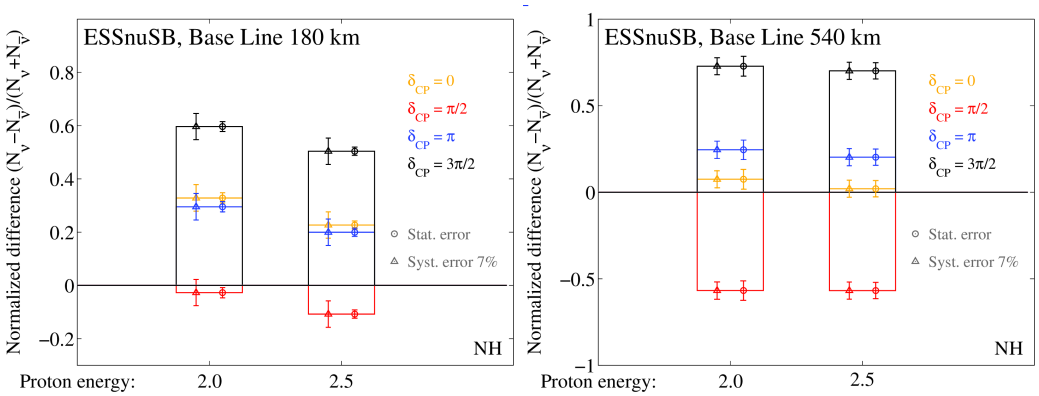

Figure 7: The bars show the normalised difference between the total numbers of electron neutrinos and of electron antineutrinos (Nν_e - N$\overline{\nu}_e$)/(Nν_e +N$\overline{\nu}_e$) for a proton energy of 2.0 GeV and 2.5 GeV, respectively, at the first maximum (180 km, left panel) and the second maximum (540 km, right panel).

(and 3.0) GeV as compared to 2.0 GeV. The systematic errors used to produce these plots are those shown in the right column (SB Opt.) of table 3 [20].

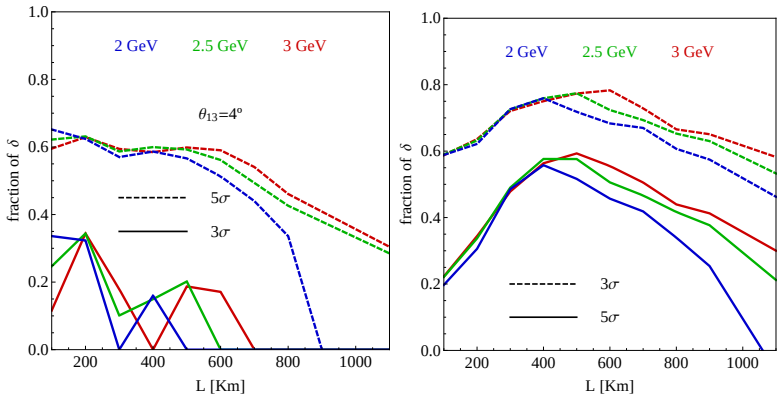

Figure 8: The curves show the fraction of the total range of possible values for δ_{cp} for which CP violation can be discovered with 5σ and 3σ significance level, respectively, as function of the distance L between the accelerator and the detector (the base line) L between 100 km to 1000 km (horizontal axis) for three different proton beam energies 2.0, 2.5 and 3.0 GeV (blue, green and red curves) and for two different values of the mixing angle $\theta_{13} = 4^\circ$ (left panel) and $\theta_{13} = 8.73^\circ$ (right panel). The systematic errors used to produce these plots are those listed in table 3.

With the exceptionally high power of the ESS linac it is possible to profit from the significantly higher sensitivity to δ_{cp} at the second maximum, rendering ESSnuSB about 3 times less sensitive to systematic errors as compared to experiments measuring at the first maximum.

Fig. 9 shows, for ESSnuSB using a 540 km baseline and a proton energy of 2.0 GeV (left panel, current ESS design) and 2.5 GeV (right panel, originally planned linac energy for which upgrade space is available in the linac tunnel), respectively, the dependance of the fraction of values of δ_{cp} for which a CP violation discovery at 5σ and 3σ, respectively can be made as a function of event statistics, or, as it is called in this figure, "exposure". The "nominal exposure" corresponds to 10 years of data taking, 2 years with a neutrino beam and 8 years with an antineutrino beam. The systematic errors that have been used are shown in the right column (SB Opt.) of table 3. The upper boundary of the colored bands assumes the neutrino hierarchy to be known and the lower

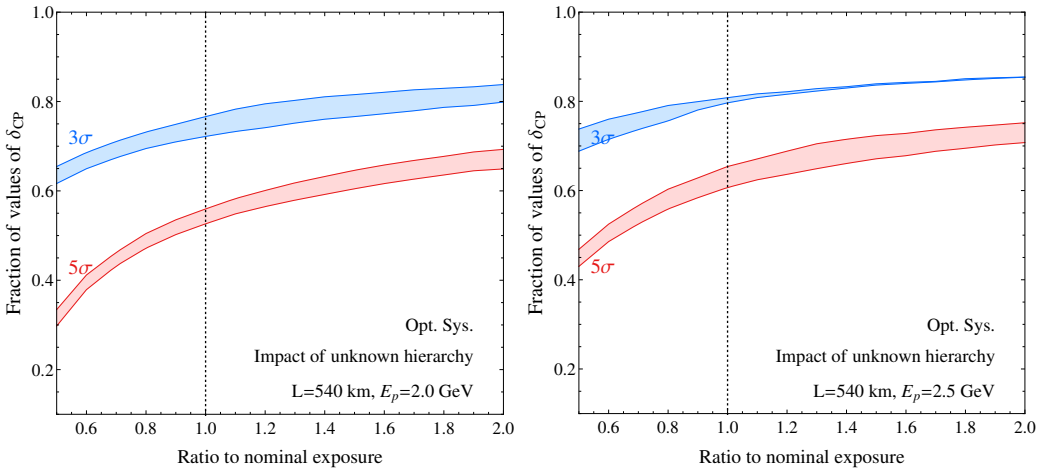

Figure 9: Curves showing the dependence of the fraction of values of δ_{cp} for which a CP violation discovery at 5σ and 3σ, respectively, can be made as a function of event statistics, or exposure, where the nominal exposure corresponds to 10 years of data taking. The left panel is for a proton energy of 2.0 GeV (current ESS design) and the right panel for 2.5 GeV (originally planned linac energy for which upgrade space is available in the linac tunnel). The upper boundaries of the colored bands were obtained assuming the hierarchy to be known (NH) and the lower boundaries assuming the hierarchy to be unknown, i.e. it is marginalized over. The systematic errors used to produce these plots are those shown in the right column (SB Opt.) of table 3 [20].

boundary to be unknown. For the nominal exposure, assuming the neutrino hierarchy to be known, CP violation can be discovered at 5σ in about 56% and 65% of the total range of possible values, for a 2.0 GeV and a 2.5 GeV linac proton energy, respectively. Doubling the exposure to 4 years with a neutrino beam and 16 years with an antineutrino beam will lead to an increase of the fraction of the total range of possible δ_{cp} covered to 69% and 71%, respectively.

The comparatively small difference between this fraction assuming the hierarchy to be known and unknown, illustrates the comparatively weak dependence on this parameter at the low neutrino energies of ESSnuSB.

Assuming a 2% signal systematic error for DUNE and a 5% signal systematic error for Hyper-K, these experiments would cover only of the order of 10% of the range of possible CP violation angle values as illustrated in Fig. 10. These two experiments could only reach the same level of performance for CP discovery and measurement as ESSnuSB if their systematic signal errors could be reduced to the level of 2-3% for for Hyper-K and 1% for DUNE, which as of today remains an empirically unproven assumption.

The larger reach of ESSnuSB is confirmed by global calculations, made by the theory group at the Snowmass Study in the US 2013 [8], in which were compared the expected performances of the different proposals for international neutrino beam projects, using the same systematic errors for all experiments, in this case the systematic errors shown in the left column (SB Def.) of table 3. In the left panel of Fig. 11 is shown the 1σ error in the determination of δ_{cp} (horizontal axis) as a function of the covered fraction ofδ_{CP} (vertical axis). One can see that among the accelerator based projects shown, the resolution attainable with ESSnuSB is surpassed only by the Neutrino Factory project (IDS-NF). The right panel shows with which level of significance, in terms of number of standard deviations σ, CP violation can be discovered (vertical axis) versus the fraction of the total range of possible values for δ_{cp} for which CP violation (horizontal axis) can be discovered. From these plots ESSnuSB can be seen to have the widest discovery coverage of the δ_{cp} range among the Super Beam experiments investigated.

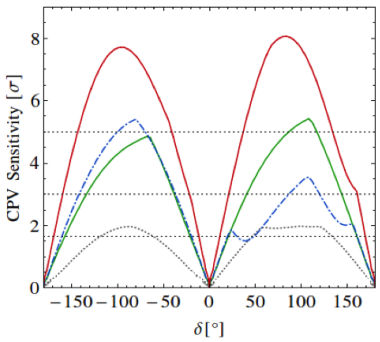

Figure 10: Curves showing the significance in terms of standard deviations σ for discovery of leptonic CP violation (vertical axis) as a function of the CP violating angle δ_{cp} in the range $-180\,^\circ$ to $+180\,^\circ$ (horizontal axis) for ESSnuSB (red curve), LBNF/DUNE (green curve) and Hyper-K (blue curve). The systematic errors used on the signal and the background rates are 5% and 10% for T2HK and ESSnuSB and 2% and 5% for LBNF/DUNE. [21]. An unknown mass hierarchy is assumed.

3 The required upgrades and additions to the ESS accelerator facility

Since at ESS (unlike at the US Spallation Neutron Source (SNS) [28]) the accelerated protons will be sent directly from the ESS linac to the neutron spallation target the spallation neutron pulses will be of will be of approximately the same length as the 2.86 ms long proton pulses in the linac. The requirement to have μs short pulses on the target for neutrino production makes it necessary to compress the proton pulses using an accumulator ring. The injection of many turns into this ring cannot be made efficiently if the injected beam consists of the same particles as the circulating beam. By accelerating H^- ions in the linac, an efficient injection system can be designed based on the use of stripping foils or a laser beam, thus producing a circulating proton beam in the accumulator. This requires that the linac is made such that it can accelerate interleaved pulses of protons and H^-. In particular the linac magnets must be designed such that it will be possible to switch between two different optics settings for the two different linac beams.

A second ion source for the production of H^- will thus be needed, as well as a duplication of the equipment in the H^- injector line up to the point where the H^- beam line is merged with the proton linac. The optimal place for merging the two lines remains to be identified, on the basis of the beam transport efficiency from the source.

H^- ions in the linac beam will lose electrons due to phenomena such as collisions with residual gas, with blackbody photons, and by intra-beam stripping. This will lead to some additional beam loss which needs to be minimized. Lorentz stripping in the magnetic fields can be reduced by careful choice of the optics for the H^- beam. The maximally allowed beam loss for both beams together, H^- and H^+, is 0.1 W/m. This limit has to be guaranteed by good design of the transport of the H^- beam and by the collimation system.

The H^- linac pulse will need to be chopped in the Medium Energy Beam Transport Line (3.6 MeV) to have regular gaps in the pulse such that the length from the beginning of one gap to the beginning of the next corresponds to the circumference of the accumulator. This is needed in order to avoid beam spilling at injection into the accumulator, for radio frequency beam capture in the accumulator and for the extraction of the beam to the production target. These gaps are seen by the accelerating cavities in the linac and the resulting higher order resonance modes (HOMs) may excite the beam and cause beam loss that needs to be minimized. The fact that there is no beam in the gaps represents a loss of about 10 % of the particles on the production target.

The baseline energy of the linac beam is 2.0 GeV with contingency space available in the linac tunnel for upgrade to higher energies. As mentioned in section 2, higher energies are beneficial for the physics reach of

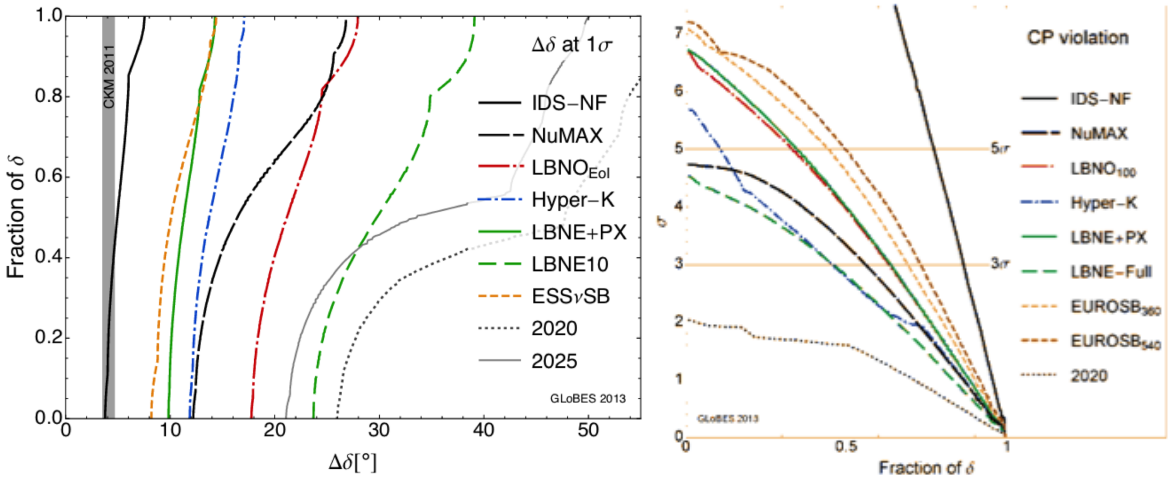

Figure 11: In the left panel the 1σ error in the determination of δ_{cp} is shown (horizontal axis) as a function of the δ_{CP} fraction for which this accuracy can be reached (vertical axis) [22]. The right panel shows with what level of significance in terms of number of standard deviations σ that leptonic CP violation can be discovered (vertical axis) versus the fraction of the total range of possible values for δ_{cp} (horizontal axis) [3]. The systematic errors used to produce these plots are those shown in the left column (SB Def.) of table 3.

the ESSnuSB facility. The accumulator will be designed in a way to make it possible to profit from a future linac upgrade. The extraction will be made in the contingency region of the linac tunnel, see Fig. 1, at a point where higher energies can be reached by adding more accelerating modules. Due to space limitations around the neutron target hall the transfer line from the linac to the accumulator cannot be designed for a beam energy higher than 2.5 GeV. This limitation is due to the requirement that the radius of the H^- beam transfer lines must be large enough for the Lorentz stripping to be within the allowed margins for radiation. With a 66% dipole filling factor in the transfer line and 2.5 GeV beam energy, the radius must not be smaller than about 110 m [25]. A first layout for the accumulator, the target, the transfer lines, and the neutrino beam direction is shown in Fig. 12. The target station would need to be located at a depth of 25 m for radio-protection reasons and the neutrino beam will therefore pass below the proton linac.

There are several additional important items in the inventory of upgrades that need to be made during the linac construction phase for the future additional 5 MW H^- beam, such as the extra infrastructure and space that will be required for additional cabling and electrical equipment, for extra power transformers, for the additional H^- source and for the beam equipment of the H^- beam transport at low energy. The water cooling plant, the cryogenic liquids plant, the cooling channels in the radio frequency power sources and the accelerating cavities need to be designed for increased dynamic heat load. The tetrode radio frequency sources for the spoke cavities need to have water-cooled screen-grids. The klystron modulators for the elliptical cavities need to be of the modular type to allow for the future upgrade of the average power and the repetition rate [14]. Furthermore it has to be possible to change the strengths of the linac focussing and steering magnets with the linac pulsing frequency. It is essential that these comparatively modest preparatory modifications be made during the linac build-up phase 2017-2023 to reduce the cost and time required for the subsequent linac upgrade and in particular to reduce the disruption in the linac operation for neutron production to an acceptable level.

Error source	SB Def.	SB Opt.
Fiducial Volume ND	0.5%	0.2%
Fiducial Volume FD	2.5%	1.0%
Flux error signal ν	7.5%	5%
Flux error background ν	15%	10%
Flux error signal $\bar{\nu}$	15%	10%
Flux error background $\bar{\nu}$	30%	20%
Background uncertainty	7.5%	5%
Cross secs x eff. QE	15%	10%
Cross secs x eff. RES	15%	10%
Cross secs x eff. DIS	7.5%	5%
Effec. ratio ν_e/ν_μ QE	11%	3.5%
Effec. ratio ν_e/ν_μ RES	5.4%	2.7%
Effec. ratio ν_e/ν_μ DIS	5.1%	2.5%
Matter density	2%	1%

Table 3: The different sources of uncertainty that contribute to the total systematic uncertainty in the determination of the CP violating angle δ_{cp} . This table is an extraction of information from a table used in (NF)[24]. Here only the uncertainties for the Super Beam cases "SB Def." (for Default) used to obtain the results shown in Fig. reffig10 and "SB Opt." (for Optimistic) used to obtain the results shown in Figs 8, 10 and 11

3.1 The Accumulator

To fill the accumulator ring with as much as $1.1 \cdot 10^{15}$ protons is a challenging task. This number could be reduced by splitting the 2.86 ms linac pulse in shorter and more frequent linac pulses of the same current, and the 5 MW total power for the neutrinos [26]. To give an example, to have one pulse, 2.86 ms long, for neutrons and 4 pulses, 0.72 ms long, for neutrino production, would reduce the number of protons in the accumulator to 1/4, but increase the pulsing rate of the linac to 70 Hz, see the lower part of figure 13. The neutron pulse frequency would still be 14 Hz. Alternatively, the 2.86 ms pulse could be injected into four stacked accumulators [8]. In either way, one quarter, of the number of protons would be accumulated in the ring. First studies are ongoing to optimize a lattice layout of an accumulator with 376 m circumference and 1.32 μs revolution time. The baseline is to have one accumulator ring. Studies will show how many particles can be stored in the accumulator, and this will give the necessary linac pulsing frequency. Having only one ring, needs careful design of the stripping foil, which has to accept higher pulse rates than in the case of four stacked rings. The option with four rings is subject to Lorentz stripping in the switchyard, which distributes the linac beam into the four rings. Beam loss from this beam distribution would have to be evaluated and taken into account [27].

Increasing the number of pulses leads to increased power consumption in the cavities because of the power losses when ramping up and down the radio frequency field strength in the cavities for each pulse. 5 MW beam power needs 13.3 MW wall plug power for 14 pulses of 2.86 ms per second. In the case of one accumulator ring and 70 Hz pulse frequency (see figure 13) 13.3 MW + 17.0 MW wall plug power will be needed. The cost of the additional 3.7 MW will have to be weighed against the cost of the construction, the power consumption, the operation of 3 additional accumulators and the impact on the target pulsing. On the other hand, the injection foil in one accumulator will have to strip four times as many particles as in the case of the four-ring option, implying more severe requirements on the foil. Ongoing testing and future operational experience will show how many pulses per second can be handled. The choice of linac pulsing has impact also on the powering and pulsing of the target focussing system.

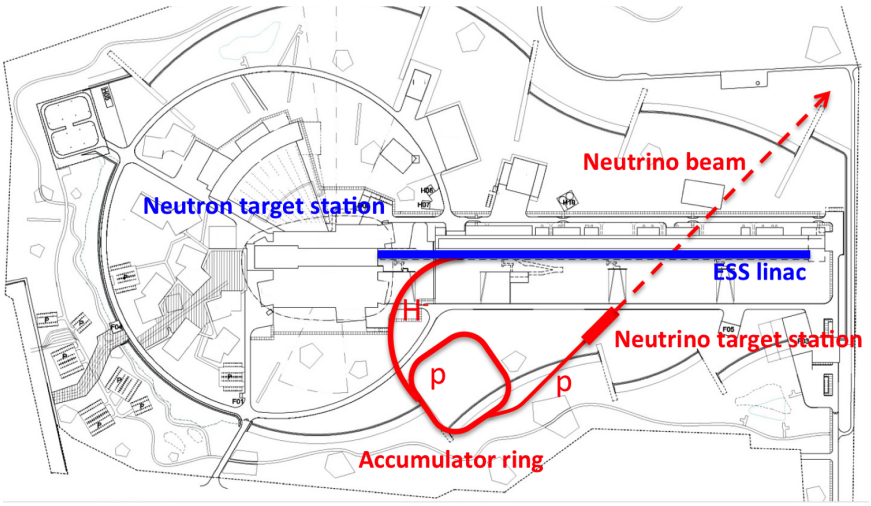

Figure 12: Proposed layout on the ESS site (courtesy K. Hedin, ESS). The beam in the accumulator and the transfer lines, the neutrino target station and the neutrino beam are shown in red, the linac beam in blue.

3.1.1 Lattice

To store $3 \cdot 10^{15}$ protons in the accumulator requires a well chosen magnetic fields structure (the lattice). The circumference and the beam pipe aperture are critical; the cost of investment and operation of the accumulator will critically depend on its design. The design concept of the accumulator ring at the SNS, in which the magnet fields in the original 1 GeV lattice are rather moderate, has been used as a starting point for the design of the ESSnuSB accumulator. It is possible to adopt the SNS 30 m injection straight sections unchanged for 2 GeV. However, in view of the large apertures required, the bending fields in the arcs are kept as conservative as in the SNS; hence the arc lengths have tentatively been doubled considering that collective effects are more important at lower energies and that this would be conservative for 2.5 GeV. The circumference is increased from 248 to 376 m, which reduces the number of injection turns per fill. The SNS collimation layout in the first long straight section after the injection section has so far been kept the same [28].

Different lattice types will be designed to study space charge effects. The first simulations have been made using the SNS FODO lattice [26]. A FODO lattice is flexible and robust and gives a compact beam size for high energy machines with, however, a relatively large variation around the ring in the transverse beam size [29]. Doublet lattices give more space in the lattice and are optimal for focusing of highly non-spherical beams (mini-β in electron colliders) and can lead to large variations in the transverse beam size. Triplets give a smooth variation of the beam size, and, in particular, small variations of the ratio between the two transverse sizes, (e.g. small β in p-colliders) and an almost uniformly distributed space-charge field.

3.1.2 Injection

For the first step in the design procedure a total final charge in the accumulator of 1/4 of the original $1.1 \cdot 10^{15}$ protons, corresponding to a 2.86 ms pulse length, has been assumed, implying about 1000 injected turns. This intensity gives tune shifts of 0.2 [8]. The accumulator radio frequency system will keep the protons confined in an rf "bucket" and prevent the protons to fill the gap in the circulating beam in such a way that the beam can be extracted with low beam loss. As mentioned above, this gap will be generated in the linac medium energy section by chopping a part of the pulse corresponding to the gap duration. This is repeated with the accumulator

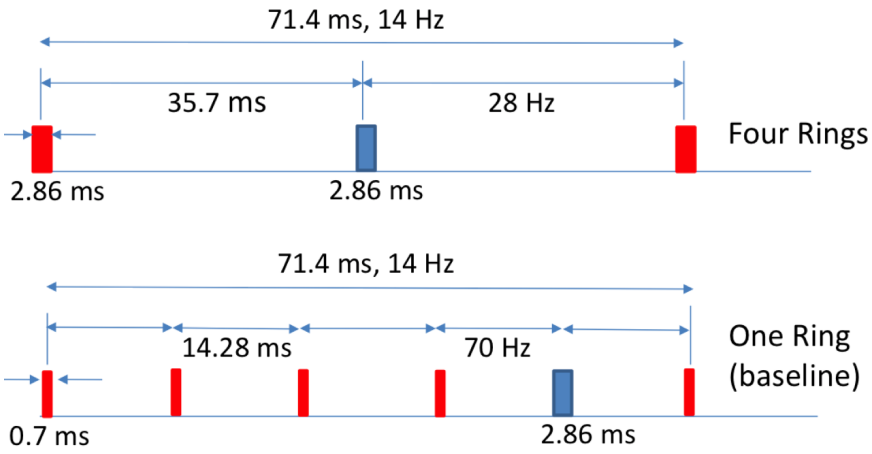

Figure 13: Pulse distribution for the case with four stacked accumulators and for the one-ring options: The upper part of the figure shows the 28 Hz pulsing of the linac with one proton (blue) and one H^- (red) pulse interleaved and the lower part shows the case of four 0.72 ms long pulses of H^- for neutrinos are followed by one 2.86 ms proton pulse for the neutrino spallation target. The upper case needs a switching system and empty spaces in the H^- pulse to distribute the particles in the four stacked rings.

revolution frequency along the linac pulse. The gap duration will be determined by the extraction kicker rise time which is between 50 and 100 ns, the exact value depending on the design of the lattice and the angle of extraction.

Just like at the SNS, we propose, as a first implementation, charge exchange injection by foil stripping since this technology is well known. Ultimately, laser stripping is envisaged, and, although no design exists so far, tests are ongoing [30]. A future SNS laser stripping realization could ultimately be ported to the ESS accumulator with limited modifications, provided the SNS-like injection lattice is kept for the ESSnuSB accumulator design.

The injection process is being studied by tracking particles from the linac using the ESS linac beam parameters derived from simulations. The idea is to "paint" the phase space at injection in a way such as to minimize space charge effects, while keeping a limited beam size. After the 1000 turns injection the beam will be extracted to the target.

Stripping foil temperatures were computed with the use of several different methods [26, 31, 32]. A peak temperature of 2050 K at the hottest spot is produced under the combined effect of the linac beam and the circulating beam (the incident linac beam alone heats to 1800 K). Although this may be considered as tolerable according to present experience, it would be safer to reduce the peak temperatures to a level for which operational experience exists, like at the SNS, where temperatures do not exceed 1600 K. The average number of foil passes per particle was found to be approximately 4.5.

The obvious way to reduce the foil temperature is by increasing the spot size of the incoming H^- beam. The lattice matching conditions require that a blow-up of the transverse size of the circulating beam be only local. This can be achieved by modifying the optics of the injection straight section and adding correction quadrupoles in the remaining straight sections to conserve the tunes. Changing the optical beta function values (β_x, β_y) at the foil from (-9.4, 19.5) m to (18.4, 51.6) m, was found to widen the circulating beam by 40% in x and 62% in y, respectively, and to lower the peak temperatures down to 1440 K for the incident linac beam alone and to 1550 K for the the H^- and H^+ beams together, in both cases with about the same average number 4.8 of foil passes. These simulations show that with 100 π (95%) normalized emittance, foil temperatures can be kept at acceptable levels, with the hottest spots at 1650 K.

For a fully injected beam in the accumulator having a normalized emittance of 200 π, filling the ring with two linac pulses of 1.5 ms instead of four pulses of 0.7 ms, simulations show that peak temperatures of 1560 K for the H^- beam alone and 1850 K for the sum of the effect of H^+ and H^- beams are reached. The maximum space charge tune shifts remain below -0.16, which is a clearly acceptable value. The temperature profile on the foil for this case is shown in Fig.14.

The final beam emittance in the ring will be chosen so as to permit efficient extraction of the beam from the accumulator and guiding of the beam through the switchyard [33] from the accumulator to the four targets, still keeping the temperature of the foil within limits.

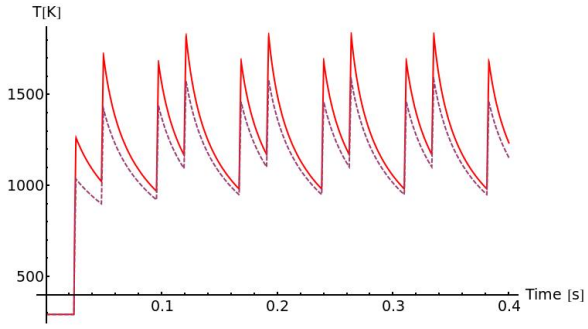

Figure 14: Evolution of maximum foil temperatures [K] at the H^-- spot peak (dashed) and the combined H^- and circulating protons peak (red). Only two injections into the accumulator per linac pulse.

4 Design Considerations for the Near Detector

To achieve the required experimental sensitivity it will be important to construct a Near Detector (ND) located close to the neutrino production point. The required performance of the ND is that it should enable measurements of the flux of each neutrino species in the beam directly after production, along with the respective cross sections, to a precision better than 5%. As the electron neutrino content in the beam is $\sim 0.3\%$, the ND needs to be able to separate Charged Current (CC) muon and electron neutrino events on a level better than 10^{-4}. The cross section depends on the neutrino energy so the ND needs to provide an energy measurement. These requirements need to be satisfied to keep the systematic uncertainty below the statistical uncertainty for the ESSnuSB.

The ND design considerations discussed below concern a cylindrical water Cherenkov detector with its central axis aligned with the neutrino beam direction. It has a radius of $R_{\rm ND} = 5$ m, length of $L_{\rm ND} = 10$ m, is placed at a depth of 21 m and at a distance of $z_{\rm ND} = 500$ m from the target station. On the outside it is covered with scintillator plates to veto atmospheric muons and to reject events not fully contained in the detector. Further details on the study of this and other ND designs can be found in [34].

The input to the study was a neutrino beam profile obtained using FLUKA 2011.xx (version 2014) [35] and GEANT 3.21 [36]. The calculation was made with a proton beam energy of 2 GeV, implying that the neutrino energy distribution is as shown in Fig. 3, and with the horn focused positively charged particles. The beam neutrinos were then used to simulate neutrino interaction events in water with the GENIE toolkit [37].

The angular acceptance of the FD is $\sim \pm 0.1$ mrad, while for the ND it is $\sim \pm 10$ mrad. As the ND provides the baseline for the Far Detector (FD) measurements, it is important that the neutrino energy spectrum and beam flavour composition at the two detector points are not significantly different . It was checked that when the angle with respect to the beam axis of the produced neutrinos varies from 0 to 10 mr, the change in neutrino flavour composition and energy distribution is indeed negligible.

For the ND located at $z_{\text{ND}} = 500$ m with a radius $R_{\text{ND}} = 5$ m and length $L_{\text{ND}} = 10$ m the muon neutrino CC event rate would be ~ 260 s^{-1} and the electron neutrino CC event rate would be ~ 1 s^{-1}. For the total CC event rate of the two neutrino flavors and a neutrino beam pulse frequency of 14 Hz and pulse width of ~ 1.5 μs, the average temporal separation of the beginnings of two subsequent events is ~ 80 ns. The total required collection time of the produced Cherenkov light of one event is ~ 30 ns, i.e. of the same order of magnitude as the average time separation of two events. This means that it is not unlikely for two neutrino interactions to overlap in time, thereby complicating the event reconstruction.

For ESSnuSB neutrino energies the muons resulting from CC collisions travel less than 3 m in water (and the CC electrons travel less than the muons) before they stop radiating Cherenkov light. This implies that most of the events will be fully contained within the cylindrical ND water volume. Due to the comparatively low energy of the ESSnuSB neutrino beam, the majority of muons and electrons are produced close to perpendicularly to the incoming neutrino beam. The majority of the Cherenkov rings are therefore projected onto the mantle of the detector tank, as opposed to the downstream end-plate, which implies that increasing L_{ND} would not substantially reduce the precision of the reconstruction. If required, one may therefore increase L_{ND} in order to increase the count rate.

To explore the conditions for the event reconstruction an event sample was produced containing idealized neutrino CC event products in a simplified detector environment. Each event in this sample was initiated with a charged lepton placed at the origin of the coordinate system with a pre-determined kinetic energy and momentum along the z axis. A photo-detector wall was placed in the x-y plane at $z = 5$ m, where each photon is registered on impact. From the timing and position of the detected photons one can determine the position of the initial vertex, the direction of the charged lepton, its flavor and its energy.

To determine the event vertex coordinates an algorithm was developed that iteratively investigates a number of coordinate sets in the detector using the timing and positions of the detected photons. This is done with an increasingly finer granularity, and the final most probable vertex position is identified as the vertex position of the event. As the time and position coordinates of each detected photon is used, this algorithm directly ties the accuracy of the vertex position estimation to the time and position resolution of the photo-detectors. Using photo-detectors with order 0.1 ns time resolution and order 1 cm position resolution this algorithm can locate the vertex with an accuracy of a few cm.

From the simulations it was found that the energy of the lepton could be estimated from the number of detected photons, N_γ. N_γ is assumed to be roughly proportional to $E_{kin} - E_{ChTh}$, where E_{kin} is the kinetic energy of the lepton and E_{ChTh} is the threshold energy for Cherenkov light production. This threshold is derived from the mass of the lepton and the refractive index of the water, so the lepton flavor must be known.

The lepton flavor identification is done by examining the fuzziness of the edge of the produced Cherenkov ring. In order to do this, the location of the detected ring must be determined first. For this purpose an algorithm was developed as a modification of the Circular Hough Transform [38], used in image analysis to find circles (see [34]). It was found that using filled circles instead of ring contours yields a much more precise result, as the Cherenkov rings detected here are quite fuzzy objects.

The lepton flavor identification is done by using this algorithm to fit both a 'muon ring' and an 'electron ring' to the detected photons of each event and determining which flavor is most probable to have produced the Cherenkov light. To determine which flavor is the most probable, the algorithm looks at several parameters and awards each event a number of μ-votes and e-votes. These votes describe how well each event resembles a typical muon event and a typical electron event, and by applying cuts to these votes the lepton flavor of each event is determined. This first trial identification algorithm yielded a misidentification rate of 0.3%. This is significantly larger than required and further work is thus required. All misidentified events were muons that had been identified as electrons, and were mainly found among lower energy events. Further details of the algorithm used and the results obtained can be found [34].

5 Project time schedule and cost

The aim of the presently ongoing ESSnuSB Design Study is to produce a Conceptual Design Report by 2018 to be followed by a Technical Design Report by 2020. This assumes that adequate financial support for the Design Study can be secured. Taking into account technical constraints only, the upgrade of the Linac and the construction of the Accumulator, of the Neutrino Target Station, of the Near Detector and of the Far Detector could start by 2021. The ESSnuSB build-up period is estimated to take some 7 years (dominated by the construction of the far detector) leading up to start of data taking by earliest in 2027. Taking other funding and organizational constraints into account, 2030 is a more probable date for start of data taking. A crucial prerequisite for this time schedule is that the comparatively modest modifications of the linac, that are described at the end of section 3, be made during the linac build-up period 2017-2023. To introduce the same modifications once the linac is running for spallation neutron production will be very disruptive to the neutron experiments, will take more time and be significantly more costly. The cost of the ongoing Design Study is of the order of 3 MEUR, of which 1 MEUR will be needed for investigations of the Garpenberg mine, in particular by core-drilling. The MEMPHYS Megaton Water Cherenkov Detector cost has been estimated by LAGUNA-LBNO EU FP7 Design Study to an investment cost of the order 700 MEUR. The costs of the Upgrade of the Linac, of the Accumulator and of the Target Station have been very approximately estimated at 100, 200 and 200 MEUR, respectively. By the time that the Conceptual Design Report will have been concluded in 2018, these costs will have been more accurately estimated.

6 Summary and conclusions

Leptonic CP violation potentially plays a crucial role for the explanation of matter-antimatter asymmetry in the Universe. The prime opportunity to discover and measure leptonic CP violation is offered by future Super Beam experiments studying the $\nu_\mu \rightarrow \nu_e$ oscillation. Following the discovery in 2012 of a large value of the neutrino mixing angle θ_{13}, analytical calculations show that a higher sensitivity to CP violation is obtained by measuring at the second neutrino oscillation maximum as compared to the first.

This fact has been shown in this paper by comparing directly the sensitivity to CP violation of experimental observables such as the number of detected electron neutrinos and the normalized electron neutrino-antineutrino asymmetry at the first and the second maximum, respectively. The higher sensitivity , using reasonable assumptions for systematic errors, at the second maximum is also apparent from comparisons previously made between different Super Beam projects on the basis of global simulation calculations. In view of the very high neutrino beam intensity required for measurements at the second maximum, the uniquely high power of the ESS proton driver represents a significant advantage for such measurements.

ESSnuSB is currently the only Super Beam experiment which concentrates on taking its data at the second oscillation maximum. Global calculations show that taking data with ESSnuSB with a 2.0 GeV (2.5 GeV) ESS proton beam during 10 years using the MEMPHYS Megaton Water Cherenkov Detector placed in the 1200 m deep Garpenberg mine at the second maximum, 540 km from ESS, the coverage of the range of possible CP violating angle values is 56% (65%) assuming the neutrino hierarchy to be known and the neutrino-signal systematic error to be 5%.

The generation of the neutrino Super Beam using the ESS linac will require acceleration of H^- pulses. These pulses will be interleaved with the proton pulses accelerated for neutron production in such a way that the linac will deliver a 5 MW H^- beam simultaneously with the 5 MW proton beam. The H^- beam will be injected into a 376 m circumference accumulator ring, stripping off the two electrons of each H^- ion at the entrance to the ring, by multi-turn injection and ejected from the ring by single-turn extraction, thereby obtaining a compression of the pulse length from 2.86 ms to 1.3 μs. The ejected H^- beam will be guided to a neutrino

target with a surrounding horn-type hadron collector, downstream of which there is a 25 m long pion decay tunnel. The very high current required in the horn cannot be maintained for more than the order of a μs which is what necessitates the strong compression of the linac pulse.

The accumulator ring and the target station can be installed underground on the ESS site without significant interference with the linac construction and operation. The introduction of H^- pulses in the linac and the doubling of the linac average power can to a large extent be made after the completion of the linac, as presently designed, without major interference with the linac operation provided, however, that certain comparatively modest - but crucial - preparative modifications be made to the linac already during its build-up phase 2017-2023.

The accumulator ring, which will contain an exceptionally high number of protons, represents a challenging design task, in particular its injection scheme and its ring lattice and collimation. In order to somewhat reduce the complexity of the task, the number of protons per pulse can be reduced by a factor 2 or 4, using one of two alternative schemes: by injecting more and shorter H^- pulses in the compressor ring or by splitting the long H^- pulses up on more than one compressor ring. Design work of an accumulator ring receiving in sequence four 0.715 ms long pulses after each 2.86 ms long proton pulse in the linac and of an injection stripping scheme based on foil stripping is ongoing.

The Near Detector plays a crucial role for the determination of the neutrino flux and cross-sections needed in the evaluation of the Far Detector data. The simulation of a cylindrical water Cherenkov detector, 10 m long and 5 m in radius located 500 m downstream of the target, has been used to study how such a detector could match the requirements. Methods for the determination of the position of the initial CC vertex, the direction of the charged lepton, its flavor and its energy have been designed and evaluated. The results obtained so far are encouraging but need to be worked on further to satisfy the demanding requirement of not more than 5% systematic error in the Far Detector measurements.

The current ESSnuSB Design Study is foreseen to lead to a CDR in 2018 and to a TDR in 2020. Taking into account technical constraints only, construction of all parts could start in 2021 and be completed at the earliest by 2027. The investment cost for the Far Detector is estimated to 700 MEUR and for the accelerator complex to approximately 500 MEUR.

Acknowledgement

We are grateful to E. Fernandez-Martinez and P. Coloma who have contributed with calculations and plots for the physics part of this paper, to F. Gerigk and E. Montesinos for their study and report of the modifications of the ESS linac that are required to allow simultaneous acceleration of H^+ and H^- ions at an average power of 5+5 MW and to B. Holzer, B. Goddard and M. Eshraqi for having contributed to discussion and calculations for the accelerator design.

References

[1] K. Abe, et al., T2K Collaboration, Phys. Rev. Lett. 107 (2011) 041801, arXiv:1106.2822 [hep-ex]

[2] Y. Abe, et al., DOUBLE-CHOOZ Collaboration, Phys. Rev. Lett. 108 (2012) 131801, arXiv:1112.6353 [hep-ex]

[3] J.K. Ahn, et al., RENO Collaboration, Phys. Rev. Lett. 108 (2012) 191802, arXiv:1204.0626 [hep-ex]

[4] F.P. An, et al., DAYA-BAY Collaboration, Phys. Rev. Lett. 108 (2012) 171803, arXiv:1203.1669 [hep-ex]

[5] S.Peggs, executive editor, et al.: ESS Technical Design Report, ISBN 978-91-980173-2-8

[6] An Experimental Program in Neutrino Physics, Nucleon Decay, and Astroparticle Physics Enabled by the Fermilab Long-Baseline Neutrino Facility, Letter of Intent Submitted to the Fermilab PAC, P-1062, January 5, 2015, http://www.fnal.gov/directorate/program-planning/Jan2015Public/LOI-LBNF.pdf, https://dune.bnl.gov/tmp/volume-project.pdf

[7] K. Abe et al.: Physics Potential of a Long Baseline Neutrino Oscillation Experiment Using J-PARC Neutrino Beam and Hyper-Kamiokande Prog. Theor. Exp. Phys.2015, 00000 (39 pages), DOI: 10.1093/ptep/0000000000, arXiv:1502.05199v1 [hep-ex] 18 Feb 2015

[8] E. Baussan et al.: A Very Intense Neutrino Super Beam Experiment for Leptonic CP Violation Discovery based on the European Spallation Source Linac: A Snowmass 2013 White Paper, Nuclear Physics B, Volume 885, August 2014, Pages 127-149, arXiv:1309.7022 [hep-ex]

[9] T.R. Edgecock, O. Caretta, T. Davenne, C. Densham, M. Fitton, D. Kelliher, P. Loveridge, S. Machida, Phys. Rev. ST Accel. Beams 16 (2013) 021002, arXiv:1305.4067 [physics.acc-ph]

[10] F. Gerigk, et al., Conceptual Design of the Low-Power and High-Power SPL, 2014, CERN-2014-007

[11] O. Brunner, S. Calatroni, E. Ciapala, M. Eshraqi, R. Garoby, F. Gerigk, A. Lombardi, R. Losito, et al., Phys. Rev. ST Accel. Beams 12 (2009) 070402.

[12] E. Baussan, et al., EUROnu Super Beam Collaboration, arXiv:1212.0732 [physics.acc-ph].

[13] L. Agostino, et al., MEMPHYS Collaboration, J. Cosmol. Astropart. Phys. 1301 (2013) 024, arXiv:1206.6665 [hep-ex]

[14] F. Gerigk and E. Montesinos, CERN; report 13 June 2014; Recommended modifications of the ESS baseline architecture for ESSnuSB

[15] D. McGinnis, M. Lindroos, R. Miyamoto IPAC 13, Shanghai, THPWO073

[16] LAGUNA Large apparatus studying grand unification and neutrino astrophysics, http://www.laguna-science.eu/.

[17] P. Coloma, E. Fernandez-Martinez, Optimization of neutrino oscillation facilities for large θ_{13}, arXiv:1110.4583

[18] S. Parke, Neutrinos: Theory and Phenomenology, FERMILAB-CONF-13-453-T, arXiv:1310.5992v1 [hep-ph] 22 Oct2013

[19] The GLoBES code, P. Huber, M. Lindner and W. Winter, Comput. Phys. Commun. 167 (2005) 195 [hep-ph/0407333] and P. Huber, J. Kopp, M. Lindner, M. Rolinec and W. Winter, Comput. Phys. Commun. 177 (2007) 432 [hep-ph/0701187].

[20] P. Coloma, Fermilab, private communication

[21] P. Coloma, Fermilab, plot shown at a seminar at Fermilab spring 2015

[22] A. de Gouvea et al.: Neutrinos, Intensity Frontier Neutrino Working Group of Snowmass 2013 arXiv:1310.4340 [hep-ex]

[23] A. Cervera et al.: Golden measurements at a neutrino factory, arXiv:hep-ph/0002108

[24] P. Coloma, P. Huber, J. Kopp and W. Winter: Systematic uncertainties in long-baseline neutrino oscillations for large θ_{13}, September 27, 2012, EURONU-WP6-12-5,3FERMILAB-PUB-12-509-T, IDS-NF-036, arXiv.org/pdf/1209.5973v1.pdf

[25] A. J. Jason, D. W. Hudgings and O. B. Dyck, IEEE Trans. Nucl. Sci. 28, 2704 (1981)

[26] E. Wildner et al., IPAC 14, Dresden, WEPRO117

[27] E. Bouquerel et al., IPAC 13, Shanghai, TUPWO004

[28] SNS Design Manual 2003

[29] M. Fitterer, CERN-THESIS-2013-043

[30] A. V. Aleksandrov et al., Status of Laser Stripping at the SNS, Conf.Proc. C110328 (2011) 2035-2037 PAC-2011-WEP295

[31] E. Wildner et al., IPAC 15, Richmond, Virginia, THPF100

[32] M. Martini, CERN-ACC-NOTE-2015-0005

[33] E. Bouquerel et al.,
IPAC 15, Richmond, Virginia, MOPWA017, https://jacowfs.jlab.org/conf/y15/ipac15/prepress/MOPWA017.PDF

[34] A. Burgman: A Neutrino Detector Design — A Simulation Study on the Design of the Cherenkov Near Detector of the Proposed ESSνSB, (2015), lup.lub.lu.se/student-papers/record/5466261

[35] A. Ferrari, P. R. Sala, A. Fassò and J. Ranft: Fluka — A Multi-Particle Transport Code, (2005)

[36] S. Agostinelli, et al. [GEANT4 Collaboration], Nucl. Instrum. Meth. A 506, 250 (2003)

[37] C. Andreopoulos, A. Bell, D. Bhattacharya, F. Cavanna, J. Dobson, S. Dytman, H. Gallagher and P. Guzowski, et al., Nucl. Instrum. Meth. A 614, 87 (2010), arXiv:0905.2517 [hep-ph]

[38] R. O. Duda and R. E. Hart, CACM 5, 11 (1972)